International Journal of Control and Automation
Vol.7, No.4 (2014), pp.373-384
http://dx.doi.org/10.14257/ijca.2014.7.4.34

Optimum Bistatic Angle Extraction Using Compressed Time-Frequency Feature Vectors

Sung-Jun Lee[1], Seung-Jae Lee[1], In-Sik Choi[1*] and Dae-Young Chae[2]

[1]*Department of Electronic Engineering, Hannam University, 133 Ojeong -dong, Daedeok-gu, Daejon, Republic of Korea*
[2]*3rd R&D Institute, Agency for Defense Development (ADD), Daejeon, Republic of Korea*

{radar, sensor, recog}@hnu.kr, ratmcdy@add.re.kr

Abstract

When the target of interest is determined, the transmitter and receiver positions of bistatic radar are of great importance at the aspect of radar target classification. The radar cross section (RCS) of a target varies with these positions, and the target classification performance is considerably influenced by RCS. In this study, the target classification performance using the bistatic scattering data of wire targets and scale-model targets is analyzed and compared. Time-frequency analysis and effective compression techniques are used for target feature extraction from the bistatic scattering data of each target, and a multilayered perceptron (MLP) neural network is used as a classifier. The optimum receiver position is found by comparing the calculated classification probabilities while changing the position of the bistatic radar receiver. The classification results using calculated data and measured data show that an optimally positioned bistatic radar yields better classification results, demonstrating the importance of the positions of the transmitter and receiver for bistatic radar.

Keywords: *bistatic radar, radar cross section, target classification, optimum bistatic angle, feature extraction*

1. Introduction

Radar cross section (RCS) is a function of various parameters such as frequency, directions of incidence, target shapes, and polarization. Depending on the transmitter and receiver positions, the RCS is classified as mono-static or bistatic. When the transmitter and the receiver positions are the identical (*i.e.*, mono-static radar), the directions of incidence and scattering are identical, and the resulting RCS values are called mono-static RCS. However, when the transmitter and receiver positions are different (*i.e.*, bistatic radar), the directions of incidence and scattering are different [1, 2] and the resulting RCS values are called bistatic RCS. The concept of bistatic radar is not new. The earliest radars were of this type [3]. In recent times, bistatic radars have again attracted interest because they can be used to detect stealth or low RCS targets [4-8]. Bistatic radar may have a counter-stealth capability, since target shaping to reduce target mono-static RCS will in general not reduce the bistatic RCS [5, 9]. In addition, they have been applied to passive radar using television broadcasting transmitters [9], bistatic synthetic aperture radar (BSAR) imaging [10], and BSAR automatic

* In-Sik Choi (recog@hnu.kr) is the corresponding author of this paper.

ISSN: 2005-4297 IJCA

target recognition (ATR) [11-13]. However, there has not been much research about radar target classification using bistatic radar.

RCS contains useful information for radar target classification, such as scattering centers and natural resonance frequencies. The scattering centers on the target are related to the early-time response and natural resonance frequencies of the target are related to the late-time response. The early-time response occurs while the field passes across the target, whereas the late-time response occurs after the field completely passes across the target [14]. The scattering centers and natural resonance frequencies are used as feature vectors for radar target classification. We use time-frequency transforms to extract these feature vectors simultaneously.

In this work, we use the calculated bistatic scattering data of four different wire targets and the measured bistatic scattering data of three scale-model targets while changing the receiver position, and extract feature vectors using the short time Fourier transform (STFT) and continuous wavelet transform (CWT) with effective compression techniques. Then, a multilayered perceptron (MLP) neural network is used as a classifier. Using this process, the receiver position having the best performance may be found by comparing the calculated classification probabilities.

2. Proposed Method

2.1. Optimum Bistatic Angle Extraction

The general bistatic target classification process is shown in Figure 1.

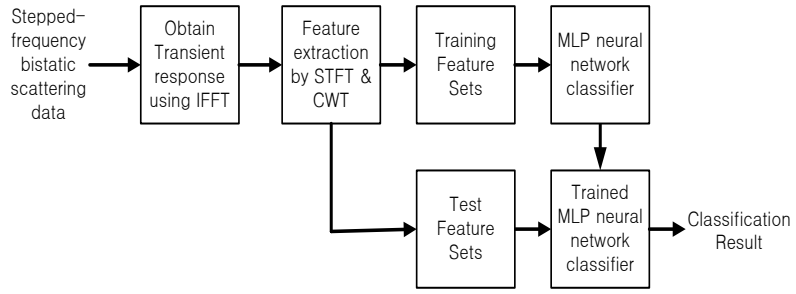

Figure 1. Process of bistatic target classification

In this paper, we propose the optimum bistatic angle extraction for radar target classification using this process. We assume that the targets of interest and radar operating frequency are determined previously. The proposed algorithm is as follows:

Step 1. Bistatic scattering data in the frequency domain are calculated using an electromagnetic simulation tool or measured using a bistatic measurement system. We assume that the transmitter Tx is located at 0° and the receiver positions are changed from Rx 1 to Rx *Kn* with a uniform interval, where *Kn* is the total number of receiver positions (Figure 2). At each bistatic angle, the targets are also rotated from 0° to a specific aspect angle limit.

Step 2. The transient response of the target is then obtained by performing an inverse Fourier transform (IFT) of the stepped-frequency bistatic scattering data.

Step 3. We extract feature vectors from the transient response using the compressed STFT and CWT matrices. The detailed feature extraction methods are explained in the following sections.

Step 4. The feature vectors are divided into training sets and test sets. The training feature vectors are used for training the MLP neural network classifier. The trained neural network provides the classification result for the test feature sets.

Step 5. At each bistatic angle, we repeat from step 2 to step 4 and obtain the target classification results. We compare the classification results of all bistatic angles, and the bistatic angle which has the best classification result is determined as the optimum bistatic angle for target classification.

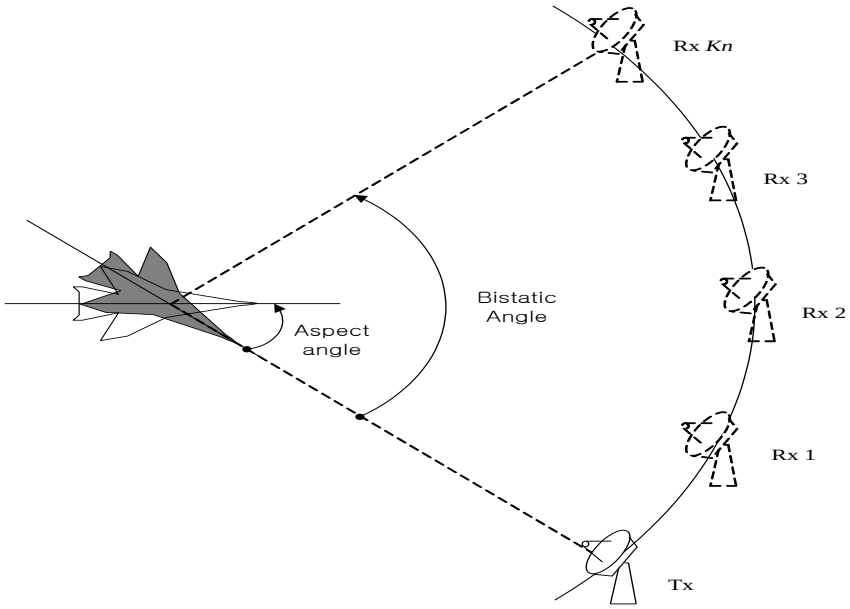

Figure 2. The configuration for calculation of bistatic scattering data

2.2. Feature Extraction Using Short-time Fourier Transform

The STFT is a basic method that is commonly used to analyze non-stationary signals such as radar signals [15, 16] and in biomedical signal processing [17]. To perform the STFT, the signal is divided into small segments, which can be assumed to be stationary. For this purpose, a Gaussian window function is chosen. Because the size of the STFT window is fixed, the resolution is also fixed. The window size must be suitably chosen for a given purpose because the time resolutions are inversely related to the frequency resolutions for a fixed window size. The STFT is defined in the time domain as follows:

$$\mathrm{STFT}(\tau,\Omega) = \int_{-\infty}^{\infty} f(t)w(t-\tau)\exp(-j\Omega t)dt \qquad (1)$$

where *f(t)* is a time domain signal and *w(t)* a window function.

From the given frequency domain scattering data, we obtain the transient response *f(t)* using the inverse fast Fourier transform (IFFT). Then, an *M* x *N* STFT matrix of *M* frequency points and *N* time points is computed using equation (1). However, an *M* x *N*

matrix is too large to act as the input of a neural network classifier. Consequently, some form of data reduction is required [18]. For this purpose, we employ the following procedure. First, the STFT matrix is divided into J time bands and K frequency bands by considering the time and frequency resolutions. The component of the feature matrix in the k^{th} frequency band and j^{th} time band is denoted as $F_{k,j}$, and is defined as

$$F_{k,j} = \int_{(j-1)\Delta_\tau}^{j\Delta_\tau} \int_{(k-1)\Delta_\Omega}^{\Delta_\Omega} \mathrm{STFT}(\tau,\Omega) d\Omega d\tau,$$

$$\text{for} \quad k = 1,\ldots,K \text{ and } j = 1,\ldots,J \quad (2)$$

where

$$\Delta_\tau = \frac{T_{final}}{J} \text{ and } \Delta_\Omega = \frac{BW}{K} \quad (3)$$

Here Δ_τ and Δ_Ω are the width of each time and frequency band, with T_{final} and BW being the final time and bandwidth, respectively.

Through this process, an M x N STFT matrix can be compressed into a K x J feature matrix. The final feature vector of K x J dimension is represented by

$$X = [F_{1,1}, F_{1,2}, \ldots, F_{1,J}, F_{2,1}, F_{2,2}, \ldots, F_{K,J-1}, F_{K,J}]^T \quad (4)$$

We used these feature vectors as the input of the neural network classifier. An M x N STFT matrix is illustrated in Figure 3(a), and a compressed K x J feature matrix is illustrated in Figure 3(b).

2.3. Feature Extraction Using Continuous Wavelet Transform

The CWT was developed to overcome the resolution problem encountered with the STFT. The transient response of a target generally contains the specular return in the early-time response and resonances in the late-time response. In order to extract this information simultaneously, it is desirable to use good time resolution in the early-time stage and good frequency resolution in the late-time stage. For this purpose, we use the CWT of a frequency signal, defined as [19]:

$$\mathrm{CWT}_f(\phi,\Omega) = \sqrt{\tau}\int F(\omega)\Psi(\tau(\omega-\Omega))d\omega, \quad (5)$$

where $\Psi(\omega)$ is the mother wavelet. It plays a similar role to that of the window function in the STFT. However, unlike the case of the STFT, the window size is not fixed, and the wavelet has characteristics with frequency variations such as contraction, expansion, and shift. We used the Morlet wavelet as the mother wavelet because it is very convenient for extracting scattering mechanisms. To use transient response data, we transform equation (5) into a time-domain integral form using the Fourier inversion:

$$\mathrm{CWT}_f(\tau,\Omega) = \frac{1}{2\pi\sqrt{\tau}}\int f(t)\psi\left(-\frac{t}{\tau}\right)e^{-j\Omega t}dt, \quad (6)$$

Here $f(t)$ and $\psi(t)$ are the IFT of $F(\omega)$ and $\Psi(\omega)$, respectively. An M x N $\mathrm{CWT}_f(\tau,\Omega)$ matrix is obtained by sampling equation (6), but we need to reduce the size of the feature matrix as in the case of STFT. To do so, we divide the entire time span into early-time ($0 < t < t_L$) and late-time ($t > t_L$) stages, where the beginning of the late-time stage (t_L) is twice the maximum transit time of the target [18]. The early-time stage is divided into J_e time bands and K_e frequency bands. In this stage, because the time resolution has to be better than the frequency resolution, J_e is greater than K_e. The component of the feature in the k_e^{th} frequency band and the j_e^{th} time band is denoted as F_{k_e,j_e}, and is defined as

$$F_{k_e,j_e} = \int_{(j_e-1)\Delta_\tau^e}^{j_e\Delta_\tau^e}\int_{(k_e-1)\Delta_\Omega^e}^{k_e\Delta_\Omega^e} \mathrm{CWT}_f(\tau,\Omega)d\Omega d\tau,$$

$$\text{for} \quad k_e = 1,\ldots K_e \text{ and } j_e = 1,\ldots, J_e \quad (7)$$

where

$$\Delta_\tau^e = \frac{t_L}{J_e} \quad \text{and} \quad \Delta_\Omega^e = \frac{BW}{K_e}. \qquad (8)$$

As with the early-time stage, we divide the late-time stage into J_l time bands and K_l frequency bands. However, in this case, K_l is greater than J_l to obtain a better frequency resolution than time resolution. The component of the feature in the k_l^{th} frequency band and the j_l^{th} time band is denoted as F_{k_l,j_l}, and is defined as

$$F_{k_l,j_l} = \int_{(j_l-1)\Delta_\tau^l}^{j_l\Delta_\tau^l}\int_{(k_l-1)\Delta_\Omega^l}^{k_l\Delta_\Omega^l} \mathrm{CWT}_f(\tau,\Omega)d\Omega d\tau,$$

$$\text{for} \quad k_l = 1,\ldots K_l \text{ and } j_l = 1,\ldots, J_l \quad (9)$$

where

$$\Delta_\tau^l = \frac{T_{final} - t_L}{J_l} \quad \text{and} \quad \Delta_\Omega^l = \frac{BW}{K_l}. \qquad (10)$$

Using the above process, an M x N $\mathrm{CWT}_f(\tau,\Omega)$ matrix is matrix is compressed into a K_e x J_e early-time feature matrix and a K_l x J_l late-time feature matrix. The final feature vector of (K_e x J_e + K_l x J_l) dimension is represented by

$$X = [X_e; X_l] \qquad (11)$$

where $X_e = [F_{1,1}, F_{1,2},\ldots, F_{1,J_e}, F_{2,1}, F_{2,2},\ldots, F_{K_e,J_e-1}, F_{K_e,J_e}]^T$ and $X_l = [F_{1,1}, F_{1,2},\ldots, F_{1,J_l}, F_{2,1}, F_{2,2},\ldots, F_{K_l,J_l-1}, F_{K_l,J_l}]^T$. The compressed $\mathrm{CWT}_f(\tau,\Omega)$ feature matrix is illustrated in Figure 3(c).

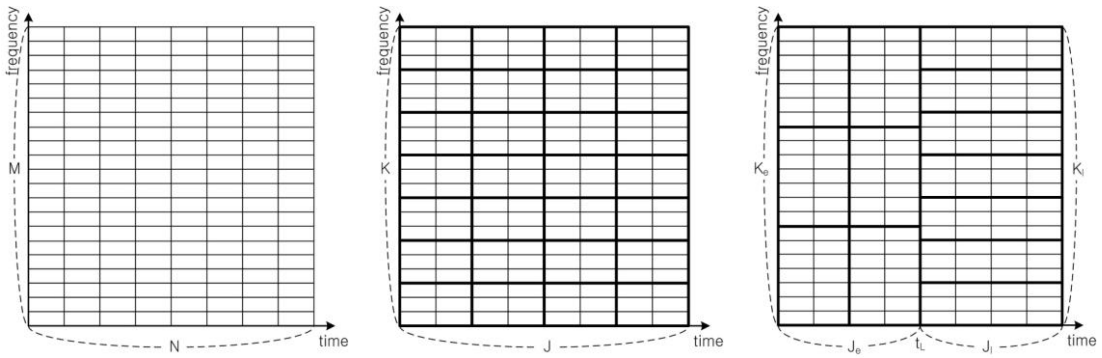

(a) M x N matrix (b) compressed STFT feature vector of K x J dimension (c) compressed CWT feature vector of K_e x J_e + K_l x J_l dimension.

Figure 3. Compression of feature vector dimension

3. Simulation and Measurement Results

To analyze the radar target classification performance of the bistatic scattering data, we first used simulation data of four different wire targets. Figure 4 shows the stick-aircraft target geometries used in the simulations. Targets A and B, as well as C and D, have the same length, but different wing angles.

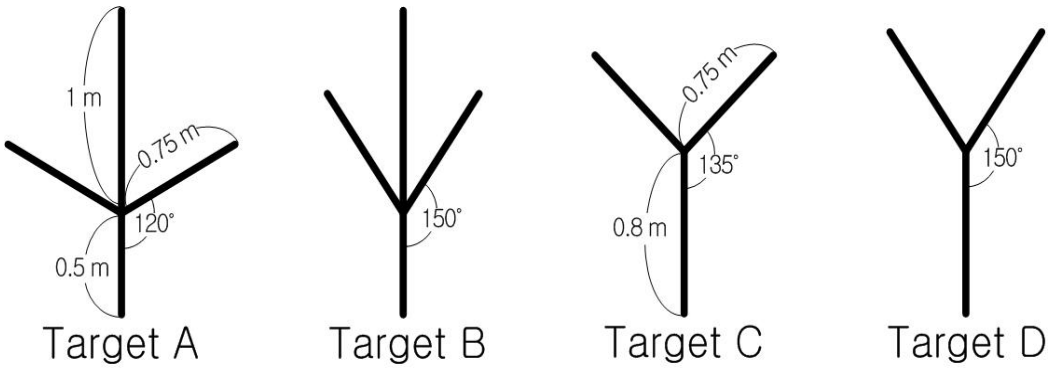

Figure 4. Targets used in the simulation

To obtain the scattering field we used the method of moments (MoM) option in FEKO. FEKO is a commercial EM simulation tool, and is based on a 3D grid. The frequency range was chosen as 7.8125 MHz to 1 GHz, with 128-point samplings and with HH polarization. The nose of wire targets is placed at the position (0,0,0), and the wire targets are placed in the x-y plane. The bistatic scattering field was calculated for each aspect angle of a counterclockwise rotated target from 0° to 150° using a 1° aspect angle step, where the transmitter was located at 0° and the receiver was located at a specific bistatic angle. Using the above process, the bistatic scattering field of 0° ~ 150° aspect angles was calculated for the receiver positions 15°, 30°, 45°, 60°, 75°, 90°, 105°, 120°, 135°, 150°, 165° to compare the target classification performance for each receiver position.

Next, feature vectors were extracted for each target using compressed STFT and CWT matrixes. First, STFT matrices of 128 x 128 dimension were constructed. In the STFT process, the window size was chosen as 15 *ns*. Then, the matrices were compressed to 8 x 8 = 64 dimensions so that they could be effectively used as the input of the MLP neural network classifier. Unlike in the case of the STFT, the time span of CWT was divided into the early-time ($0 < t < t_L$) and late-time ($t > t_L$) stages, with t_L = 10 *ns*. The dimensions during early and late-time stages were compressed to 4 x 8 and 8 x 4, respectively. Therefore, the final feature vector had 32 + 32 = 64 dimensions with the CWT.

Then, the targets were classified using an MLP neural network with two hidden layers [20]. The number of neurons in the first hidden layer was chosen to be half of the feature vector dimension, and that in the second hidden layer was chosen as one-third of that in the first hidden layer. We obtained the feature vectors at aspect angles of 0°~150° for each target. Aspect angles for the training data are from 1° to 149° with a 2° increment, and those for the test data are from 0° to 150° with a 2° increment.

Therefore, we have 75 data sets for training, and 76 data sets for testing for each target. White Gaussian noise at a given SNR was also added to the original signal of all targets. The noisy signal was used for training to make the classifier robust to noise [21]. To guarantee the classifier performance, we trained it until the mean square error (MSE) was 10^{-5}. In addition, we performed 100 Monte Carlo simulations to enhance the reliability of the simulation.

Table 1(a) and Table 1(b) show the target classification percentages and standard deviation (in parenthesis) for various positions of the bistatic radar receiver using the STFT and CWT, respectively. The simulation results indicate that regardless of the receiver position, the target classification performance using the CWT feature vector is better than that using the STFT feature vector. The optimum location of the CWT feature vector is identified as the transmitter and receiver at 0° and 90°, respectively.

The optimum location of the STFT feature vector, on the other hand, is the transmitter and receiver at 0° and 150°, respectively. These results can be changed if we use other types of targets or other feature extraction techniques. As the target scattering mechanisms are very complex, it is very difficult to analyze why this combination of angles works best. But, if the targets of interest and feature extraction methods are determined, we can extract the optimum locations of transmitter and receiver for bistatic radar classification using the above process at any case.

Table 1. The target classification percentages and its standard deviation (in parenthesis) for various positions of the receiver of the bistatic radar

(a) using STFT

Location of Tx and Rx	SNR [dB] 0	5	10	15	20
Tx=0°, Rx=15°	53.4	72.9	84.3	91.7	96.0
	(2.5)	(2.0)	(1.7)	(1.3)	(1.0)
Tx=0°, Rx=30°	56.9	73.7	84.1	92.8	95.1
	(2.4)	(2.2)	(1.7)	(1.4)	(1.0)
Tx=0°, Rx=45°	57.5	72.1	86.0	92.7	96.6
	(2.4)	(2.3)	(1.9)	(1.4)	(0.8)
Tx=0°, Rx=60°	62.9	81.8	91.7	97.4	98.6
	(2.3)	(1.7)	(1.2)	(0.7)	(0.6)
Tx=0°, Rx=75°	66.2	83.4	93.0	96.6	98.8
	(2.0)	(1.6)	(1.1)	(0.8)	(0.5)
Tx=0°, Rx=90°	70.9	86.2	92.0	96.5	98.2
	(2.0)	(1.4)	(1.1)	(0.8)	(0.7)
Tx=0°, Rx=105°	68.1	87.2	94.8	97.1	98.1
	(2.1)	(1.6)	(1.0)	(0.8)	(0.7)
Tx=0°, Rx=120°	69.3	86.4	93.4	96.8	97.6
	(2.2)	(1.5)	(1.1)	(0.7)	(0.6)
Tx=0°, Rx=135°	64.5	84.2	94.3	97.2	97.9
	(2.5)	(1.6)	(1.0)	(0.6)	(0.6)
Tx=0°, Rx=150°	70.8	87.6	95.5	98.2	99.0
	(2.6)	(2.1)	(0.8)	(0.5)	(0.4)
Tx=0°, Rx=165°	67.0	85.6	94.8	97.3	98.7
	(2.7)	(1.5)	(1.0)	(0.6)	(0.4)

(b) using CWT

Location of Tx and Rx	SNR [dB] 0	5	10	15	20
Tx=0°, Rx=15°	74.7	89.1	96.7	98.6	99.5
	(1.8)	(1.5)	(1.0)	(0.6)	(0.3)
Tx=0°, Rx=30°	75.2	89.4	96.4	98.5	99.5
	(1.9)	(1.4)	(0.9)	(0.4)	(0.3)
Tx=0°, Rx=45°	71.3	89.3	95.9	98.7	99.6
	(2.3)	(1.4)	(0.8)	(0.5)	(0.3)
Tx=0°, Rx=60°	77.0	92.1	97.9	99.2	99.5
	(2.0)	(1.3)	(0.7)	(0.4)	(0.2)
Tx=0°, Rx=75°	83.1	94.2	98.6	99.4	99.5
	(1.8)	(1.2)	(0.5)	(0.3)	(0.2)
Tx=0°, Rx=90°	85.9	95.6	99.3	99.6	99.8
	(1.5)	(1.0)	(0.4)	(0.3)	(0.1)
Tx=0°, Rx=105°	83.1	95.1	98.4	99.4	99.7
	(2.2)	(0.9)	(0.6)	(0.3)	(0.2)
Tx=0°, Rx=120°	80.5	95.2	97.4	99.2	99.4
	(2.0)	(0.9)	(0.6)	(0.3)	(0.2)
Tx=0°, Rx=135°	80.6	94.7	98.1	99.0	99.3
	(2.0)	(1.2)	(0.6)	(0.3)	(0.2)
Tx=0°, Rx=150°	83.6	93.9	98.8	99.4	99.4
	(2.2)	(1.1)	(0.5)	(0.3)	(0.3)
Tx=0°, Rx=165°	81.5	94.3	98.0	98.7	99.1
	(2.1)	(1.1)	(0.5)	(0.3)	(0.2)

In the second example, we applied the proposed method to the data measured using the Michigan State University (MSU) arch range, which is a bistatic measurement system. The measurement configuration is shown in Figure 5. Scattering targets are placed on a low density styrofoam column, which is at the center of the arch range, at the same height as the horn antennas from the ground to provide the most uniform incident field. The frequency-domain measured data were obtained for a frequency range of 2 GHz ~ 5.81 GHz with a 30 MHz step increment. Aspect angles varied from 0°~30° with respect to the nose, at 0.5° intervals. The bistatic angles between transmitter horn and receiver horn are 12.4°, 30° and 60°. Three different targets (F-22, F-14 and B-58) of 1:32 scale shown in Figure 6 are used for measurement.

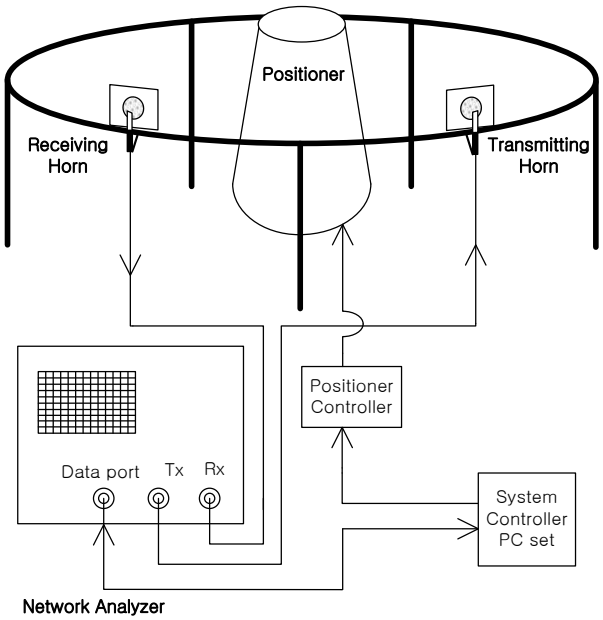

Figure 5. Bistatic radar measurement system at MSU

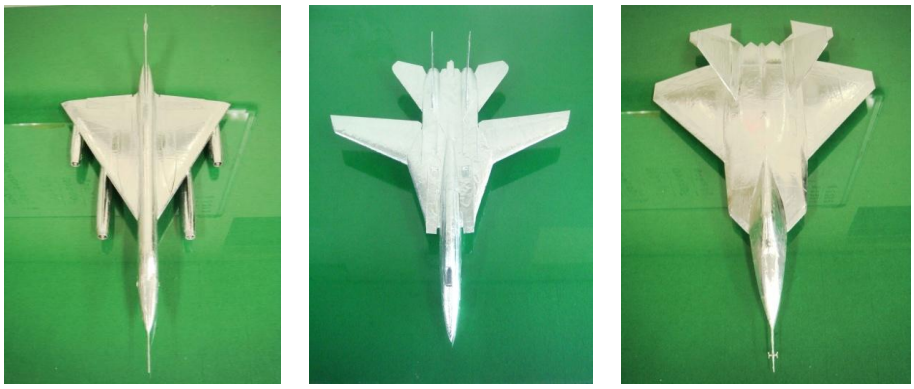

(a) B-58 (b) F-14 (c) F-22

Figure 6. Scale model targets used for measurement

Then, we extract feature vectors for each target using compressed STFT and CWT matrices. The original STFT matrixes are 128 x 128 dimension, and were compressed to 8 x 8 = 64 dimensions. Similarly, the original CWT matrixes are 128 x 128 dimension and were compressed to 4 x 8 and 8 x 4 during the early- and late-time stages, respectively. The MLP neural network with two hidden layers is used as the classifier. Aspect angles for the training data are from 0.5° to 29.5° with a 1° increment, and those for the test data are from 0° to 30° with a 1° increment. 100 Monte Carlo simulations are performed and the means and standard deviations are obtained.

Table 2(a) and 2(b) show the target classification percentages and standard deviation (in parenthesis) for three receiver positions of the bistatic radar using the STFT and CWT, respectively. The results show that the STFT is slightly better than the CWT feature vectors, and the optimum location of both the STFT and the CWT feature vectors is identified as the transmitter and receiver at 0° and 60°. This result is different from that of the wire targets. Since the bistatic scattering fields are changed with the

target shapes and operating frequency, the optimum bistatic angle for target classification is also changed with respect to the targets and operating frequency used. Therefore, we can apply our method to the placement of the bistatic transmitter and receiver when the targets of interest, operating frequency and feature extraction method are determined.

Table 2. The measured target classification percentages and its standard deviation (in parenthesis) for three receiver positions of the bistatic radar

(a) using STFT

Location of Tx and Rx	SNR [dB] -10	-5	0	5	10
Tx=0°, Rx=12.4°	36.16 (4.21)	49.85 (5.05)	72.03 (3.54)	87.71 (2.98)	94.73 (1.53)
Tx=0°, Rx=30°	38.85 (4.78)	44.72 (4.33)	61.13 (4.40)	73.46 (3.38)	89.01 (2.49)
Tx=0°, Rx=60°	45.26 (4.71)	68.28 (4.42)	80.11 (3.04)	90.43 (2.87)	95.24 (1.29)

(b) using CWT

Location of Tx and Rx	SNR [dB] -10	-5	0	5	10
Tx=0°, Rx=12.4°	35.96 (4.48)	49.70 (4.23)	68.37 (4.20)	86.32 (2.86)	97.23 (1.28)
Tx=0°, Rx=30°	35.61 (4.44)	45.77 (4.76)	63.67 (4.52)	76.80 (3.04)	88.31 (2.69)
Tx=0°, Rx=60°	39.09 (4.20)	58.61 (4.31)	77.98 (3.60)	91.83 (2.36)	95.45 (1.45)

4. Conclusion

In this paper, target classification performance using bistatic scattering field for four different wire targets and three different scale model aircraft targets is analyzed. The compressed STFT and CWT time-frequency techniques were used for feature vector extraction from the bistatic scattering field of each target, and an MLP neural network was used as a classifier.

For CWT feature vector, the optimum location of the transmitter and receiver were found to be at 0° and 90° for wire targets and 0° and 60° for the scale model targets, respectively. The optimum location for the STFT feature vector, on the other hand, is the transmitter and receiver at 0° and 150° for wire targets and 0° and 60° for scale model targets, respectively.

Consequently, we can decide where the transmitter and receiver should be located in the bistatic radar when the targets, operating frequency and feature extraction techniques are determined. Future work will include simulations with more realistic targets and additional measured bistatic scattering data for other feature extraction methods.

Acknowledgements

This work was supported by the Basic Science Research Program through the National Research Foundation of Korea (NRF) funded by the Ministry of Education (No. NRF-2012R1A1A4A01009094). This work has been also supported by the "Sensor Target Recognition Laboratory (STRL)" program of Defense Acquisition Program Administration and Agency for Defense Development.

References

[1] J. I. Glaser, "Some Results in the Bistatic Radar Cross Section(RCS) of Complex Objects", Proceedings of the IEEE, vol. 77, no. 5, **(1989)**, pp. 639-648.
[2] A. B. Blyakman, and I. A. Runova, "Forward Scattering Radiolocation Bistatic RCS and Target Detection", IEEE Radar Conference, Waltham, MA, **(1999)**, pp. 203-208.
[3] M. Cherniakov, "Bistatic Radar: Principles and Practice", John Wiley & Sons Ltd., **(2007)**.
[4] L. Gürel, H. Bagci, J. C. Castelli, A. Cheraly and F. Tardivel, "Validation through Comparison: Measurement and Calculation of the Bistatic Radar Cross Section of a Stealth Target", Radio Science, vol. 38, no. 3, **(2003)**, pp. 1046-1058.
[5] H. D. Griffiths, "Bistatic and Multistatic Radar", IEE Military Radar Seminar, Shrivenham, UK, **(2004)**.
[6] R. J. Boyle and W. Wasylkiwskyj, "Comparison of Monostatic and Bistatic Bearing Estimation Performance for Low RCS Targets", IEEE Trans. Aerospace and Electronic Systems, vol. 30, no. 3, **(1994)**, pp. 962-968.
[7] X. F. Li, Y. J. Xie and R. Yang, "Bistatic RCS Prediction for Complex Targets using Modified Current Marching Technique", Progress In Electromagnetics Research, vol. 93, **(2009),** pp. 13-28.
[8] E. G. Alivizatos, M. N. Petsios and N. K. Uzunoglu, "Towards a Range-doppler UHF Multistatic Radar for the Detection of Non-cooperative Targets with Low RCS", Journal of Electromagnetic Waves and Applications, vol. 19, no. 15, **(2005)**, pp. 2015-2031.
[9] C. Wei, and W. Chang, "System Level Investigations of Television Based Bistatic Radar", Master Thesis, University of Cape Town, **(2005)**, pp. 14-15.
[10] M. Cherniakov, "Space-surface Bistatic Synthetic Aperture Radar-prospective and Problems", Proc. RADAR 2002 Conference, Edinburgh, UK, **(2002)**, pp. 22-25.
[11] A. K. Mishra and B. Mulgrew, "Bistatic SAR ATR", IET Radar, Sonar & Navigation, vol. 1, no. 6, **(2007)**, pp. 459-469.
[12] A. K. Mishra and B. Mulgrew, "Ground Target Classification for Airborne Bistatic Radar", EMRS DTC Technical Conference, Edinburgh, **(2004)**.
[13] N. K. Ibrahim, R. S. A. Raja Abdullah and M. I. Saripan, "Artificial Neural Network Approach in Radar Target Classification", Journal of Computer Science, vol. 5, no. 1, **(2009)**, pp. 23-32.
[14] E. M. Kennaugh, "Opening Remarks", IEEE Trans. Antennas and Propagation, vol. 29, no. 2, **(1981)**, pp. 190-194.
[15] E. J. Rothwell, K. M. Chen and D. P. Nyquist, "An adaptive-window-width Short-time Fourier Transform for Visualization of Radar Target Substructure Resonances", IEEE Trans. Antennas and Propagation, vol. 46, no. 9, **(1998)**, pp. 1393-1395.
[16] H. Ling, J. Moore, D. Bouche and V. Saavedra, "Time-frequency Analysis of Backscattered Data from a Coated Strip with a Gap", IEEE Trans. Antennas and Propagation, vol. 41, no. 8, **(1993)**, pp. 1147-1150.
[17] M. Akay, "Time-frequency and Wavelets in Biomedical Signal Processing", IEEE Press, Chicago, America, **(1997)**.
[18] I. S. Choi and H. T. Kim, "Efficient Feature Extraction from Time-frequency Analysis of Transient Response for Target Identification", Microwave and Optical Technology Letters, vol. 26, no. 6, **(2000)**, pp. 403-407.
[19] H. Kim and H. Ling, "Wavelet Analysis of Radar Echo form Finite-size Targets", IEEE Trans. Antennas and Propagation, vol. 41, no. 2, **(1993)**, pp. 200-207.
[20] I. S. Choi, D. K. Seo, J. K. Bang and H. T. Kim, "Radar Target Recognition using One-dimensional Evolutionary Programming–Based CLEAN", Journal of Electromagnetic Waves and Applications, vol. 17, no. 5, **(2003)**, pp. 763-784.
[21] S. Chakrabarti, N. Bindal and K. Theagharajan, "Robust Radar Target Classifier using Artificial Neural Network", IEEE Trans. Neural Network, vol. 6, no. 3, **(1995)**, pp. 760-766.

Authors

Sung-Jun Lee

Sung –Jun Lee received B.S. and M.S. degrees in Electronic Engineering from Hannam University, Daejeon, Korea, in 2010 and 2012, respectively. His research interests include radar signal processing and radar system design

Seung-Jae Lee

Seung-Jae Lee received B.S. and M.S. degrees in Electronic Engineering from Hannam University, Daejeon, Korea, in 2011 and 2013, respectively. He is now pursuing Ph.D. program in Electronic and Information Communication Engineering from Hannam University. His research interests include radar signal processing and radar system design

In-Sik Choi

In-Sik Choi received B.S. degree in Electrical and Electronics Engineering from Kyungpook National University, Daegu, Korea in 1998 and M.S. and Ph.D. degrees in Electrical and Electronics Engineering from Pohang University of Science and Technology (POSTECH), Pohang, Kyungpook, Korea in 2000 and 2003, respectively. From 2004 to 2007, he worked at Agency for Defense Development(ADD) as a senior research engineer. He is now a Professor in Department of Electronic Engineering, Hannam University, Daejeon, Korea. His research interests include Radar signal processing, RCS measurements and RFID.

Dae-Young Chae

Dae-Young Chae received B.S. degree in Electronics Engineering from Sungkyunkwan University, Suwon, Kyunggi Province, Korea in 2006 and M.S. degrees in Electrical and Electronics Engineering from Pohang University of Science and Technology (POSTECH), Pohang, Kyungpook, Korea in 2008. From 2008, he has been worked at Agency for Defense Development(ADD) as a senior research engineer. His research interests include Radar signal processing, RCS measurements and NCTR.